Article

Co-Precipitation Synthesis and Optical Properties of Mn^{4+}-Doped Hexafluoroaluminate w-LED Phosphors

Tim Senden * [ID]**, Robin G. Geitenbeek and Andries Meijerink**

Condensed Matter and Interfaces, Debye Institute for Nanomaterials Science, Utrecht University, P.O. Box 80000, 3508 TA Utrecht, The Netherlands; r.g.geitenbeek@uu.nl (R.G.G.); a.meijerink@uu.nl (A.M.)
* Correspondence: t.senden@uu.nl; Tel.: +31-30-253-2214

Abstract: Mn^{4+}-activated hexafluoroaluminates are promising red-emitting phosphors for white light emitting diodes (w-LEDs). Here, we report the synthesis of Na$_3$AlF$_6$:Mn^{4+}, K$_3$AlF$_6$:Mn^{4+} and K$_2$NaAlF$_6$:Mn^{4+} phosphors through a simple two-step co-precipitation method. Highly monodisperse large (~20 μm) smoothed-octahedron shaped crystallites are obtained for K$_2$NaAlF$_6$:Mn^{4+}. The large size, regular shape and small size distribution are favorable for application in w-LEDs. All Mn^{4+}-doped hexafluoroaluminates show bright red Mn^{4+} luminescence under blue light excitation. We compare the optical properties of Na$_3$AlF$_6$:Mn^{4+}, K$_3$AlF$_6$:Mn^{4+} and K$_2$NaAlF$_6$:Mn^{4+} at room temperature and 4 K. The luminescence measurements reveal that multiple Mn^{4+} sites exist in M$_3$AlF$_6$:Mn^{4+} (M = Na, K), which is explained by the charge compensation that is required for Mn^{4+} on Al^{3+} sites. Thermal cycling experiments show that the site distribution changes after annealing. Finally, we investigate thermal quenching and show that the luminescence quenching temperature is high, around 460–490 K, which makes these Mn^{4+}-doped hexafluoroaluminates interesting red phosphors for w-LEDs. The new insights reported on the synthesis and optical properties of Mn^{4+} in the chemically and thermally stable hexafluoroaluminates can contribute to the optimization of red-emitting Mn^{4+} phosphors for w-LEDs.

Keywords: Mn^{4+}; red emission; phosphors; white LED; hexafluoroaluminate; thermal quenching

1. Introduction

White light emitting diodes (w-LEDs) are nowadays widely applied in general lighting and consumer electronics because of their high energy efficiency and long operation lifetime [1–5]. Commercial w-LEDs generate white light by combining blue-emitting (In,Ga)N LED chips with inorganic phosphors that convert part of the blue LED emission to green, yellow and/or red light [5,6]. Currently, the typical red phosphors in w-LEDs are Eu^{2+}-doped nitrides. These phosphors can have quantum yields (QYs) exceeding 90%, but a drawback is that the Eu^{2+} emission band extends into the deep red and near-IR regions where the sensitivity of the human eye is low [6–8]. As a result, there are significant efficacy losses (reduced lumen/W output) at high color rendering indices (CRIs) when using Eu^{2+}-doped nitrides as red phosphors in w-LEDs [9]. To overcome this issue, efficient narrow band red-emitting phosphors with λ_{max} ~620 nm have to be developed.

Mn^{4+}-doped fluorides are a promising class of materials to improve the color rendering of w-LEDs while maintaining a high luminous efficacy [8–11]. Upon blue photoexcitation Mn^{4+}-doped fluorides show narrow red line emission in the 600–640 nm spectral region. Furthermore, they can have a QY > 90% and are prepared through simple wet-chemical synthesis at room temperature [8,12]. These characteristics make Mn^{4+}-doped fluorides interesting narrow band red phosphors for w-LEDs. In recent years, a large number of Mn^{4+}-activated fluorides with the general chemical formulas A$_2$MF$_6$:Mn^{4+} (A = Na, K, Rb, Cs and NH$_4$; M = Si, Ge, Ti, Zr and Sn) and BaMF$_6$:Mn^{4+} (M = Si, Ge, Ti and Sn) have been reported [11–13]. In these compounds Mn^{4+} substitutes for the M^{4+} cation that is octahedrally coordinated by six F$^-$ ions. Most work

has been done on the phosphor K_2SiF_6:Mn^{4+} (KSF) [14,15]. The Mn^{4+}-doped fluorides have excellent luminescence properties. The deep red color of the 600–640 nm Mn^{4+} emission is particularly favorable for extending the color gamut of displays, and KSF is already widely applied in displays. In lighting, large-scale application is still limited, partly hampered by issues related to thermal and chemical stability and saturation at high pump powers [14,16].

Recently, the synthesis and luminescence properties of Mn^{4+}-doped hexafluoraluminates with the compositions M_3AlF_6:Mn^{4+} (M = Li, Na, K) were reported [17–20]. The ionic radius of Mn^{4+} is similar to the ionic radius of Al^{3+} (0.53 versus 0.54 Å), and as a result, Mn^{4+} can easily substitute for Al^{3+} in fluoride hosts [17,21]. The M_3AlF_6:Mn^{4+} phosphors have potential advantages over K_2SiF_6:Mn^{4+} and other Mn^{4+}-doped fluorides. First, Na_3AlF_6 and K_3AlF_6 have a melting point of ~1000 °C and therefore have a much better thermal stability than K_2SiF_6, which already decomposes at 350–400 °C [10,22–24]. Secondly, the M_3AlF_6 compounds have a lower water solubility than K_2SiF_6, making them more chemically stable under high humidity conditions [14,25]. Thirdly, hexafluoroaluminates are already produced worldwide on a large scale, as they are used as solvents for bauxite in the industrial extraction of aluminum [26]. This may facilitate cheap large-scale production of Mn^{4+}-activated hexafluoroaluminates.

Until now, different methods have been used to synthesize M_3AlF_6:Mn^{4+} phosphors. Song et al. prepared Na_3AlF_6:Mn^{4+} phosphors via a co-precipitation method [17], while others synthesized K_3AlF_6:Mn^{4+} and K_2NaAlF_6:Mn^{4+} by cation exchange [18,19]. Furthermore, K_2LiAlF_6:Mn^{4+} was synthesized via a hydrothermal method [20]. A single convenient synthesis method for preparing M_3AlF_6:Mn^{4+} phosphors is thus so far lacking. The previous works on M_3AlF_6:Mn^{4+} have reported luminescence spectra and decay curves for different Mn^{4+} doping concentrations in the temperature range of 300 to 500 K [17–20]. However, they provided no insight into the influence of (charge compensating) defects on the luminescence spectra and quantum yield of M_3AlF_6:Mn^{4+}. Furthermore, no explanations for the thermal quenching of the Mn^{4+} luminescence were given.

In this work we report a new synthesis route for Na_3AlF_6:Mn^{4+}, K_3AlF_6:Mn^{4+} and K_2NaAlF_6:Mn^{4+} based on a simple two-step co-precipitation method. We synthesize Mn^{4+}-doped hexafluoroaluminates by initially preparing the Mn^{4+}-precursor K_2MnF_6 and then in a second step precipitating M_3AlF_6:Mn^{4+} (M = Na, K) from an aqueous HF solution containing Al^{3+}, Mn^{4+} and Na^+/K^+ ions. The presented method gives good control over the composition and homogeneity of the M_3AlF_6:Mn^{4+} phosphors. All synthesized M_3AlF_6:Mn^{4+} phosphors exhibit bright red Mn^{4+} luminescence around 620 nm. For K_2NaAlF_6:Mn^{4+} we obtain highly monodisperse and large (~20 μm) phosphor particles that exhibit narrow size and shape distributions that are superior to the size and shape distributions of other reported Mn^{4+}-doped phosphors. This makes K_2NaAlF_6:Mn^{4+} interesting for use in w-LEDs, as monodisperse, uniform and large particles are favorable for reproducible and high packing density of phosphors in w-LEDs.

We perform both room-temperature and low-temperature (T = 4 K) spectral measurements of M_3AlF_6:Mn^{4+}. The measurements at 4 K reveal that multiple Mn^{4+} sites exist in M_3AlF_6:Mn^{4+}, which was not observed in previous works on Mn^{4+}-doped hexafluoroaluminates. The formation of multiple Mn^{4+} sites can be understood from the need for charge compensation for Mn^{4+} ions on an Al^{3+} site. Further evidence for the presence of multiple sites is obtained from thermal cycling experiments, which show a change in site distribution after high temperature annealing. The charge compensation and associated defects have a large influence on the luminescence properties (e.g., quantum yield) of M_3AlF_6:Mn^{4+}.

Finally, we study the thermal quenching behavior for M_3AlF_6:Mn^{4+} by measuring the luminescence intensity as a function of temperature between 300 and 600 K. The luminescence quenching temperature we find for M_3AlF_6:Mn^{4+} is 460–490 K, which is above the operating temperature of phosphors in high-power w-LEDs. The thermal quenching is explained by thermally activated crossover from the $^4T_2$ excited state to the $^4A_2$ ground state. Furthermore, there is luminescence quenching due to non-radiative energy transfer from Mn^{4+} ions to quenching sites (defects and impurities).

2. Materials and Methods

The M_3AlF_6:Mn^{4+} (M = Na, K) phosphors were synthesized through a two-step chemical co-precipitation method. In the first step the Mn^{4+}-precursor K_2MnF_6 was synthesized and in the second step the M_3AlF_6:Mn^{4+} phosphor was prepared. Since K_2MnF_6 and M_3AlF_6:Mn^{4+} are synthesized in corrosive HF solutions, all reactions described were carried out in plastic or Teflon beakers.

2.1. Chemicals

The following chemicals were purchased from Sigma-Aldrich: $KMnO_4$ ($\geq$99.0%), KF ($\geq$99.0%), H_2O_2 (30 wt % solution, ACS reagent), $Al(OH)_3$ (reagent grade), Na_2CO_3 ($\geq$99.95%) and K_2CO_3 ($\geq$99.0%). Hydrofluoric acid (HF, 40% aqueous solution) was purchased from Riedel de Haën. All chemicals were used without any further purification.

2.2. Synthesis of K_2MnF_6

K_2MnF_6 was prepared according to the method of Bode [27,28]. $KMnO_4$ (4 g) and KF (59.5 g) were dissolved in 250 mL of a 40% HF solution. The black-purple solution obtained was stirred for 30 min and then cooled with an ice bath. Under constant cooling and stirring, a 30 wt % H_2O_2 solution was added dropwise which resulted in the gradual precipitation of yellow K_2MnF_6 powder. The dropwise addition of H_2O_2 was stopped when the reaction solution turned from purple to red-brown, indicating the formation of Mn^{4+}. The K_2MnF_6 product was isolated by decanting the red-brown solution, washing the precipitate twice with 100 mL of acetone and finally drying the precipitate at 60 °C for 5 h.

2.3. Synthesis of M_3AlF_6:Mn^{4+}

$Al(OH)_3$ (10 mmol, 0.78 g) was dissolved in 15 mL 40% HF by stirring and heating at 60 °C. After cooling down to room temperature, 0.1 mmol K_2MnF_6 (1 mol % doping concentration) was added. Simultaneously, a solution of M^+ ions (M = Na, K) in 40% HF was prepared by gradually adding M_2CO_3 or MF to 40% HF (aq) while stirring. Table 1 lists the amounts of Na_2CO_3, K_2CO_3, KF and 40% HF used for preparing the M^+/HF solutions. The M^+/HF solution was added to the Al^{3+}/Mn^{4+}/HF solution, which resulted in the precipitation of Na_3AlF_6:Mn^{4+} and K_2NaAlF_6:Mn^{4+} but not K_3AlF_6:Mn^{4+} phosphor. K_3AlF_6:Mn^{4+} was precipitated by adding 50 mL of ethanol to the mixed M^+/Al^{3+}/Mn^{4+}/HF solution (ethanol acts as anti-solvent). The synthesized phosphors were isolated by decanting the solution, washing the precipitate twice with ethanol and subsequently drying at 75 °C for 3 h. Different Mn^{4+} doping concentrations could be obtained by changing the amount of K_2MnF_6 that was used in the synthesis.

Table 1. Amounts of Na_2CO_3, K_2CO_3, KF and 40% HF (aq) used in the synthesis of M_3AlF_6:Mn^{4+} (M = Na, K).

Phosphor	Na_2CO_3	K_2CO_3	KF	40% HF
Na_3AlF_6:Mn^{4+}	15 mmol	-	-	15 mL
K_2NaAlF_6:Mn^{4+}	5 mmol	10 mmol	-	15 mL
K_3AlF_6:Mn^{4+}	-	-	40 mmol [1]	3 mL

[1] A 4:1 ratio of K:Al was used, as this gave K_3AlF_6 without impurity phases. With a 3:1 ratio, the obtained phosphor contained impurities of other crystal phases.

2.4. Characterization

Powder X-ray diffraction (XRD) patterns were measured on a Philips PW1729 X-ray diffractometer using Cu K_{α} radiation (λ = 1.5418 Å). Scanning electron microscopy (SEM) images of the phosphors were obtained using a Philips XL30S FEG microscope operating at 20 keV. The manganese concentrations in the phosphors were determined with inductively coupled plasma optical emission spectroscopy (ICP-OES)

performed on a Perkin-Elmer Optima 8300 spectrometer. For the ICP-OES measurements the M_3AlF_6:Mn^{4+} phosphors were dissolved in aqua regia.

Photoluminescence (PL) measurements were performed on an Edinburgh Instruments FLS900 fluorescence spectrometer equipped with a double 0.22 m excitation monochromator. For recording emission and excitation spectra, we used a 450 W Xe lamp as excitation source and a Hamamatsu R928 photomultiplier tube (PMT) to detect the emission. For PL measurements down to 4 K, the phosphors were cooled in an Oxford Instruments liquid helium flow cryostat. PL measurements between 300 K and 600 K were performed by heating the phosphors with a Linkam THMS600 temperature controlled stage. PL quantum yields were determined with a calibrated home-built setup which consisted of a 65 W Xe lamp, excitation monochromator, integrating sphere (Labsphere) and CCD camera (Avantes AvaSpec-2048).

3. Results and Discussion

3.1. Structural Properties

To investigate the composition, size and shape of the M_3AlF_6:Mn^{4+} (M = Na, K) phosphor particles, we used different characterization techniques such as XRD, SEM and ICP-OES. Figure 1 shows XRD patterns of the M_3AlF_6:Mn^{4+} phosphors. The XRD patterns are in perfect agreement with the reference patterns for Na_3AlF_6 (PDF 00-025-0772, red), K_2NaAlF_6 (PDF 01-072-2434, blue) and K_3AlF_6 (PDF 00-057-0227, green). No other crystal phases can be observed, which confirms that the phosphor samples are single phase.
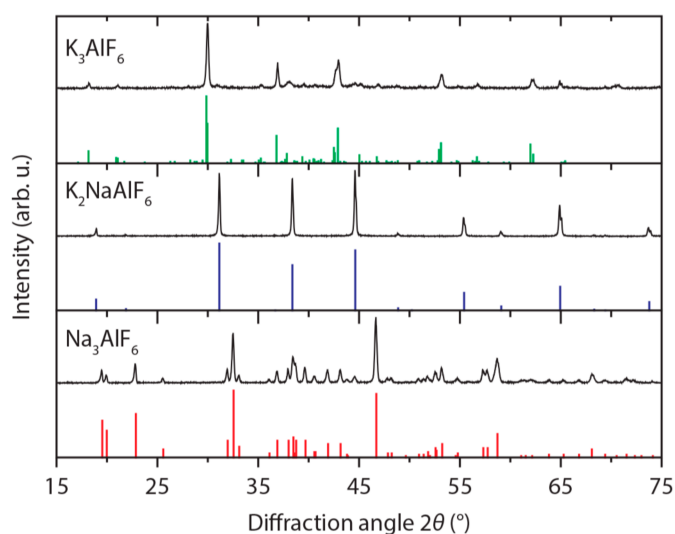
Figure 1. Powder X-ray diffraction (XRD) patterns of M_3AlF_6:Mn^{4+} (M = Na, K). The XRD patterns of the synthesized phosphors are in excellent agreement with the reference patterns for Na_3AlF_6 (PDF 00-025-0772, red), K_2NaAlF_6 (PDF 01-072-2434, blue) and K_3AlF_6 (PDF 00-057-0227, green).

The XRD measurements show that incorporation of Mn^{4+} on the Al^{3+} sites does not significantly change the crystal structure of M_3AlF_6, which is expected as the ionic radii of Mn^{4+} and Al^{3+} are similar (0.53 versus 0.54 Å) [21]. The space groups of Na_3AlF_6, K_2NaAlF_6 and K_3AlF_6 are listed in Table 2. K_2NaAlF_6 has a highly symmetric cubic crystal structure (space group is $Fm\bar{3}m$), while Na_3AlF_6 and K_3AlF_6 have a crystal structure with lower symmetry (space groups are $P2_1/n$ and $I4_1/a$, respectively) [29–31]. In the M_3AlF_6 crystal structure, the Al^{3+} ions are octahedrally coordinated by six F^- ions. Depending on the M_3AlF_6 lattice, the AlF_6 octahedron can be highly symmetric (O_h in K_2NaAlF_6) or distorted (C_i in Na_3AlF_6 and C_1 in K_3AlF_6). The average Al–F distances in the AlF_6 octahedra are around 1.8 Å.

Table 2. Space group, Al^{3+} site symmetry and average Al–F distance for M_3AlF_6 (M = Na, K); zero-phonon line (ZPL) energy of the Mn^{4+} $^2E \rightarrow {}^4A_2$ emission in M_3AlF_6:Mn^{4+}. Structural data obtained from Refs. [29–31].

Lattice	Space Group	Al^{3+} Symmetry	Al–F Distance (Å)	ZPL Energy (cm^{-1})
Na_3AlF_6	$P2_1/n$	C_i	1.808	16,167
K_2NaAlF_6	$Fm\bar{3}m$	O_h	1.778	16,082
K_3AlF_6	$I4_1/a$	C_1	1.810	16,200

By using ICP-OES, we measured the manganese concentrations in the synthesized M_3AlF_6:Mn^{4+} phosphors (see Materials and Methods section). The XRD patterns displayed in Figure 1 were measured for M_3AlF_6:Mn^{4+} phosphors containing 0.4 mol % (Na_3AlF_6:Mn^{4+}), 1.2 mol % (K_3AlF_6:Mn^{4+}) and 0.9 mol % Mn (K_2NaAlF_6:Mn^{4+}). The results presented in the rest of this work were obtained for M_3AlF_6:Mn^{4+} phosphors having these doping concentrations. For K_3AlF_6:Mn^{4+} and K_2NaAlF_6:Mn^{4+} the measured Mn concentration is very close to the 1 mol % Mn added during the synthesis, which demonstrates that our synthesis method provides good control over the Mn^{4+} doping concentration. Also a substantially higher fraction of Mn^{4+} is incorporated into K_3AlF_6 compared to previously reported cation exchange methods for preparing K_3AlF_6:Mn^{4+} [18].

Figure 2 displays SEM images of Na_3AlF_6:Mn^{4+} (0.4%), K_3AlF_6:Mn^{4+} (1.2%) and K_2NaAlF_6:Mn^{4+} (0.9%) phosphor particles. The Na_3AlF_6:Mn^{4+} (Figure 2a) and K_3AlF_6:Mn^{4+} (Figure 2b) phosphors consist of irregularly shaped particles and clusters of particles with sizes ranging from ~100 nm to >10 µm. For K_3AlF_6:Mn^{4+}, we attribute the large variety in shape and size to the rapid and forced crystallization following addition of the anti-solvent ethanol. In contrast, the synthesis of K_2NaAlF_6:Mn^{4+} (Figure 2c,d) yields highly monodisperse phosphor particles with a large average diameter of 22.5 ± 6.1 µm. The K_2NaAlF_6:Mn^{4+} particles have a smoothed octahedral shape, as expected from the cubic elpasolite structure of K_2NaAlF_6 [10,19,29]. The K_2NaAlF_6:Mn^{4+} particles prepared with our co-precipitation method have a more uniform shape and size than the K_2NaAlF_6:Mn^{4+} particles prepared by Zhu et al. via cation exchange [19]. Moreover, the K_2NaAlF_6:Mn^{4+} (0.9%) phosphor shown in Figure 2c,d exhibits particle size and shape distributions that are superior to the size and shape distributions of other reported Mn^{4+}-doped fluoride phosphors [10,24,32–37].
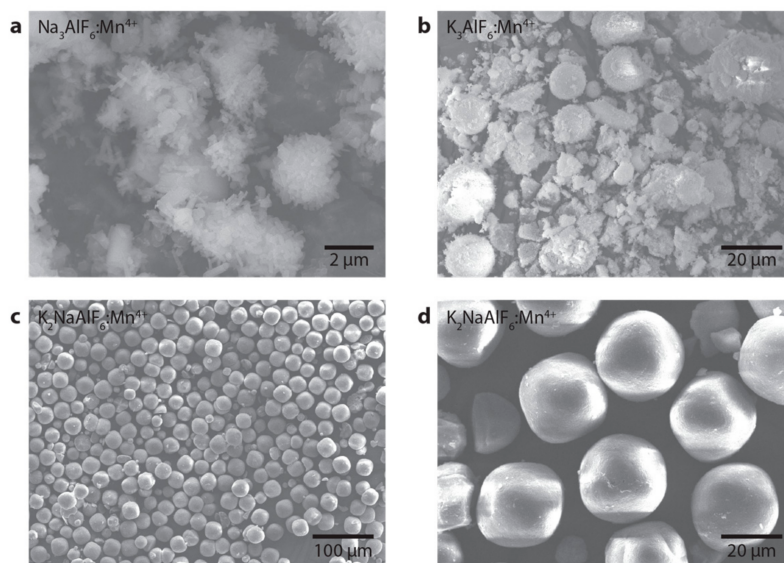
Figure 2. Representative scanning electron microscopy (SEM) images of (**a**) Na_3AlF_6:Mn^{4+} (0.4%) phosphor particles; (**b**) K_3AlF_6:Mn^{4+} (1.2%) phosphor particles and (**c**,**d**) K_2NaAlF_6:Mn^{4+} (0.9%) phosphor particles.

The high monodispersity of the $K_2NaAlF_6:Mn^{4+}$ crystallites reported here may originate from the synthesis method used. In order to achieve a narrow size distribution, it is necessary to temporally separate the particle nucleation and growth stages [38]. As described in the Materials and Methods section, we dissolve all the starting materials in HF solutions prior to the formation of the phosphor particles. Mixing of the precursor solutions results in oversaturation and the rapid formation of crystal nuclei. Once the nuclei have been formed, the precursor concentrations drop and no new nuclei are formed. The particles can grow to monodisperse and large crystallites during the growth stage. This differs from syntheses where Mn^{4+}-doped particles are prepared via cation exchange or chemical etching [14]. With these methods, new precursor ions are constantly supplied to the reaction solution preventing temporal separation of nucleation and growth.

The superior size distribution gives $K_2NaAlF_6:Mn^{4+}$ potential advantages in LED applications. Monodisperse and large crystallites are favorable for uniform and reproducible packing of phosphors, which is very important in the production of w-LEDs. In addition, phosphors with large and highly crystalline particles often display higher quantum yields because of reduced concentrations of defects which act as quenching sites. Finally, a large particle size aids the long-term stability of a phosphor.

3.2. Mn^{4+} Luminescence

Figure 3 shows the room-temperature emission and excitation spectra of $M_3AlF_6:Mn^{4+}$ (M = Na, K). Upon blue photoexcitation the Mn^{4+}-doped hexafluoroaluminates show narrow red emission lines around 620 nm (see Figure 3b). The emission lines are in a spectral range where the eye sensitivity is still relatively high, which is beneficial for applications. The red emission lines are assigned to spin- and parity-forbidden Mn^{4+} $^2E \rightarrow {}^4A_2$ transitions. Figure 3a shows that the red luminescence of $M_3AlF_6:Mn^{4+}$ has two broad excitation bands in the ultraviolet (UV) to blue spectral region. These bands correspond to the $^4A_2 \rightarrow {}^4T_1$ and $^4A_2 \rightarrow {}^4T_2$ transitions of Mn^{4+}. In all three lattices the $^4A_2 \rightarrow {}^4T_2$ excitation band is positioned at 460 nm, which indicates that the crystal field splitting is approximately equal for the investigated M_3AlF_6 hosts.
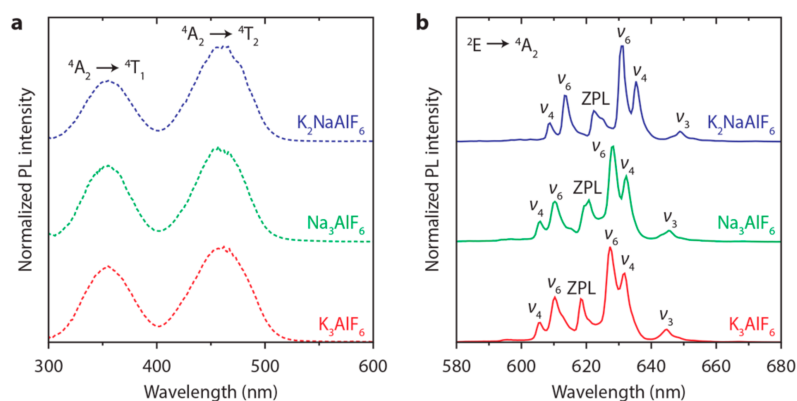
Figure 3. Room-temperature luminescence spectra of $M_3AlF_6:Mn^{4+}$ (M = Na, K) phosphors. (**a**) Excitation spectra of $K_3AlF_6:Mn^{4+}$ (1.2%) (red, λ_{em} = 628 nm), $Na_3AlF_6:Mn^{4+}$ (0.4%) (green, λ_{em} = 628 nm) and $K_2NaAlF_6:Mn^{4+}$ (0.9%) (blue, λ_{em} = 631 nm). The broad excitation bands correspond to the Mn^{4+} $^4A_2 \rightarrow {}^4T_1$ and $^4A_2 \rightarrow {}^4T_2$ transitions; (**b**) Emission spectra (λ_{exc} = 460 nm) of $K_3AlF_6:Mn^{4+}$ (1.2%) (red), $Na_3AlF_6:Mn^{4+}$ (0.4%) (green) and $K_2NaAlF_6:Mn^{4+}$ (0.9%) (blue). The Mn^{4+} emission spectra consist of zero-phonon (ZPL) and (anti-)Stokes vibronic (ν_i) $^2E \rightarrow {}^4A_2$ emission lines.

The emission spectra of $M_3AlF_6:Mn^{4+}$ in Figure 3b resemble the emission spectra observed for other Mn^{4+}-doped fluoride phosphors [33,39,40]. By analogy, the $^2E \rightarrow {}^4A_2$ emission spectra of $M_3AlF_6:Mn^{4+}$ consist of a zero-phonon line (ZPL) at ~620 nm and anti-Stokes and Stokes vibronic (ν_3, ν_4 and ν_6) lines on the high and low energy side of the ZPL, respectively [39]. The Mn^{4+} emission spectra are dominated by vibronic lines because the parity selection rule is relaxed by coupling of the

^{2}E $\to$ ^{4}A$_2$ electronic transition with odd-parity vibrations (ν_3, ν_4 and ν_6 vibrational modes) [39,41]. It is noted that the ^{2}E $\to$ ^{4}A$_2$ ZPL intensity of M$_3$AlF$_6$:Mn^{4+} is relatively strong when compared to other Mn^{4+}-doped fluorides. For example, in K$_2$SiF$_6$:Mn^{4+} the ZPL intensity is less than 5% of the Stokes ν_6 intensity, while in K$_3$AlF$_6$:Mn^{4+} the ZPL intensity is almost half of the Stokes ν_6 intensity [40]. The intense ZPL is an interesting property for (w-LED) applications, as it improves the color quality of the red Mn^{4+} phosphor. Furthermore, the observation of relatively strong zero-phonon lines is a sign that the MnF$_6$ centers lack inversion symmetry. The presence of odd-parity crystal field components relaxes the parity selection rule by inducing mixing with opposite parity states. As a result, the radiative lifetime of the ^{2}E $\to$ ^{4}A$_2$ emission is shorter (which is beneficial to reduce saturation effects) and the ^{4}A$_2$ $\to$ ^{4}T$_2$ absorption is stronger (and thus less material or a lower Mn^{4+} concentration is needed to absorb the desired fraction of blue LED light).

The strong ZPL intensity in K$_3$AlF$_6$:Mn^{4+} can be attributed to the low symmetry for Mn^{4+} on the Al^{3+} sites, i.e., the AlF$_6$ octahedron lacks an inversion center (C$_1$ symmetry, see Table 2). As discussed, without inversion symmetry, the ^{2}E $\to$ ^{4}A$_2$ ZPL intensity increases due to relaxation of the parity selection rule by odd-parity crystal field components that mix odd-parity states into the 3d wavefunctions [42]. In Na$_3$AlF$_6$ and K$_2$NaAlF$_6$ the AlF$_6$ octahedra have inversion centers (C$_i$ and O$_h$ symmetry, respectively) and the ^{2}E $\to$ ^{4}A$_2$ ZPL is expected to be weak, since there are no odd-parity crystal field components to relax the parity selection rule. The emission spectra in Figure 3b however show that the ZPLs of Na$_3$AlF$_6$:Mn^{4+} and K$_2$NaAlF$_6$:Mn^{4+} are significant, which indicates that at least for a part of the Mn^{4+} ions the site symmetry is lower than C$_i$ (no inversion symmetry). This we explain by the charge compensation required for the Mn$^{\bullet}_{Al}$ sites (the Kröger-Vink notation is used to identify defects). The proximity of charge compensating defects (probably V$'_{K,Na}$ vacancies or F$'_i$ interstitials) gives rise to local deformation of the MnF$_6$ octahedra and lifts the inversion symmetry, causing the ^{2}E $\to$ ^{4}A$_2$ ZPL intensity of Na$_3$AlF$_6$:Mn^{4+} and K$_2$NaAlF$_6$:Mn^{4+} to increase.

Besides influencing the ^{2}E $\to$ ^{4}A$_2$ ZPL intensity, the charge compensating defects have a large influence on the integrated luminescence intensity and emission lifetime of M$_3$AlF$_6$:Mn^{4+}. Typical luminescence quantum yield (QY) values measured for the M$_3$AlF$_6$:Mn^{4+} phosphors are 39% for Na$_3$AlF$_6$:Mn^{4+}, 53% for K$_2$NaAlF$_6$:Mn^{4+} and 55% for K$_3$AlF$_6$:Mn^{4+}. These QY values are below unity, which is attributed to non-radiative transfer of excitation energy from Mn^{4+} to crystal defects. At the defects the excitation energy is lost non-radiatively as heat, i.e., the defects act as quenching sites. The defect concentration will increase with the Mn^{4+} concentration, and it is therefore expected that the luminescence quenching becomes stronger at higher Mn^{4+} concentrations. Previously, it has been measured that the luminescence intensity and emission lifetime of M$_3$AlF$_6$:Mn^{4+} significantly decrease with increasing Mn^{4+} concentration already at doping levels of 4% Mn^{4+} [17–19]. In these works, the decrease in intensity and lifetime with the Mn^{4+} concentration was explained by concentration quenching, i.e., energy migration between Mn^{4+} ions to quenchers (defects, impurities). Energy migration is however not expected at doping concentrations of 4%, as most Mn^{4+} ions will not have Mn^{4+} neighbors in this concentration range (see also [43]). The results presented here indicate that quenching becomes stronger due to an increase in the defect concentration connected to the need for charge compensation and not because of enhanced energy migration among the Mn^{4+} ions.

We performed low-temperature (T = 4 K) spectral measurements to get more insight into the Mn^{4+} sites in M$_3$AlF$_6$:Mn^{4+}. In addition, the measurements at 4 K allow us to accurately compare the energy of the emitting ^{2}E level in the different M$_3$AlF$_6$ hosts. Figure 4 displays emission spectra (λ_{exc} = 460 nm) at T = 4 K of M$_3$AlF$_6$:Mn^{4+}. In line with the luminescence spectra at room temperature, the 4 K emission spectra of M$_3$AlF$_6$:Mn^{4+} consist of zero-phonon and vibronic ^{2}E $\to$ ^{4}A$_2$ emission lines (labeled ZPL, ν_3, ν_4 and ν_6). Multiple lines are observed in the ZPL region. The peaks marked with a star can be due to ^{2}E $\to$ ^{4}A$_2$ electronic transitions that couple with low energy rotatory or translatory lattice vibrational modes [40,44]. Vibronic lines due to these modes are usually found at 50–150 cm^{-1} relative to the ZPL in emission spectra of Mn^{4+}. Alternatively, the peaks marked with a star can be ZPLs of Mn^{4+} ions located on different sites than the Mn^{4+} ions yielding the most intense zero-phonon

emission line (labeled ZPL in Figure 4). Mn^{4+} emission lines caused by lattice modes are typically very weak, and therefore it is more probable that the peaks marked with stars are ZPLs of Mn^{4+} ions with other geometric environments [33,44]. In addition, multiple Mn^{4+} sites can be expected, based on the need for charge compensation. Below, further evidence is given which indicates that the various sharp emission lines around 620 nm arise from MnF_6 groups with different local geometries related to charge compensation.
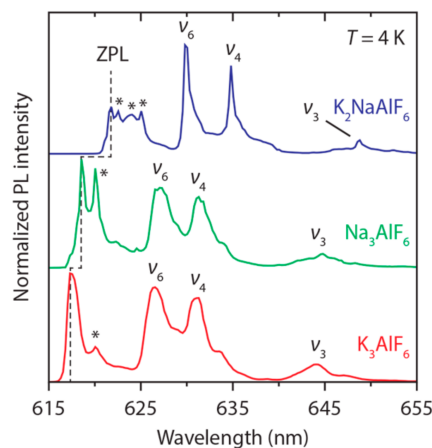
Figure 4. Emission spectra of K_3AlF_6:Mn^{4+} (1.2%) (red), Na_3AlF_6:Mn^{4+} (0.4%) (green) and K_2NaAlF_6:Mn^{4+} (0.9%) (blue) at $T = 4$ K. The excitation wavelength is 460 nm. Labels are assigned to the highest-energy zero-phonon line (ZPL) and vibronic $^2E \rightarrow {}^4A_2$ emissions (ν_3, ν_4 and ν_6). The stars mark lines assigned to ZPLs of other Mn^{4+} sites (see text).

In Figure 5 we investigate the presence of multiple Mn^{4+} sites by measuring 4 K luminescence spectra of K_2NaAlF_6:Mn^{4+} for various excitation and emission wavelengths. The excitation spectra in Figure 5a show that the structure in the $^4A_2 \rightarrow {}^4T_2$ excitation band of K_2NaAlF_6:Mn^{4+} changes significantly with emission wavelength. If only one Mn^{4+} site would be present in K_2NaAlF_6:Mn^{4+}, the excitation spectrum will have the same shape and structure for all emission wavelengths. However, here, the excitation spectrum changes significantly with emission wavelength, which indicates that more than one Mn^{4+} site is present in K_2NaAlF_6:Mn^{4+}. Furthermore, the spectra in Figure 5b show that the shape of the $^2E \rightarrow {}^4A_2$ spectrum is different for various excitation wavelengths within the $^4A_2 \rightarrow {}^4T_2$ band. This confirms that multiple Mn^{4+} sites exist in K_2NaAlF_6:Mn^{4+}, and likely also in K_3AlF_6:Mn^{4+} and Na_3AlF_6:Mn^{4+}. The presence of more than one Mn^{4+} site in M_3AlF_6:Mn^{4+} was not observed in previous reports on Mn^{4+}-doped hexafluoraluminates [17,18]. Instead, from time-resolved measurements it was concluded that only one Mn^{4+} emission site was present in M_3AlF_6:Mn^{4+}. The formation of geometrically different Mn^{4+} sites in M_3AlF_6:Mn^{4+} is expected as charge compensation is required for the $Mn_{Al}^{\bullet}$ center. The charge compensating defect can be local or distant, i.e., in the first shell of cations around the Mn^{4+} ion or further away in the lattice. A distant defect will not influence the local geometry around the Mn^{4+} ion, whereas a local defect can cause a deformation of the fluorine octahedron around the Mn^{4+} ion. This will give rise to multiple differently charge compensated Mn^{4+} sites within the lattice, depending on the type and local geometry of charge compensation.

To study the influence of the M_3AlF_6 (M = Na, K) host on the energy of the Mn^{4+} ^2E level, we compare the positions of the highest-energy $^2E \rightarrow {}^4A_2$ ZPLs in M_3AlF_6:Mn^{4+}. The energies of these ZPLs (labeled ZPL in Figure 4) are 16,200 cm^{-1} (K_3AlF_6:Mn^{4+}), 16,167 cm^{-1} (Na_3AlF_6:Mn^{4+}) and 16,082 cm^{-1} (K_2NaAlF_6:Mn^{4+}). The ^2E level energies are also listed in Table 2. The energy of the ^2E level for Mn^{4+} in M_3AlF_6 is in good agreement with the ^2E level energy observed for Mn^{4+} in other fluoride hosts [45,46]. Furthermore, it is observed that the energy of the Mn^{4+} ^2E level increases from K_2NaAlF_6 to Na_3AlF_6 to K_3AlF_6 (see dashed line in Figure 4). This indicates that the local structure

and type of M^+ cation in the second coordination sphere around the Mn^{4+} ion has an influence on the ^2E level energy. Previous studies on $M_2SiF_6:Mn^{4+}$ (M = Na, K, Rb or Cs) also show an influence of the M^+ cation on the ^2E level energy [33,40,44]. In these compounds the energy E of the ^2E level follows the trend $E(Na^+) > E(K^+) > E(Rb^+) > E(Cs^+)$, which suggests that the ^2E level energy decreases with the radius or electron affinity of the M^+ ion [21]. This is however not confirmed by our results for the $M_3AlF_6:Mn^{4+}$ phosphors, where the highest ^2E energy is found for $K_3AlF_6:Mn^{4+}$. Instead, the results in Table 2 indicate that the energy of the ^2E level increases when the Mn–F (Al–F) distance becomes longer or when the symmetry of the Mn^{4+} site (Al^{3+} site) is reduced. It is however not possible to draw definite conclusions from the data in Table 2 as the symmetry and distances in (part of) the MnF_6 octahedra will change due to deformations caused by nearby charge compensating defects.
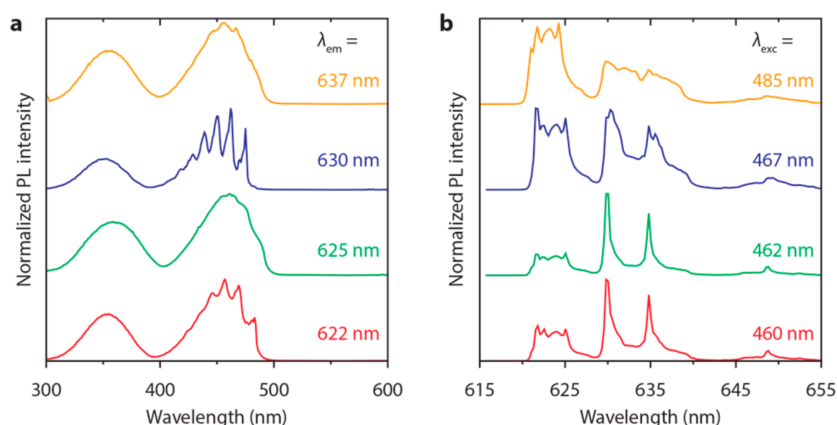
Figure 5. Emission and excitation spectra of $K_2NaAlF_6:Mn^{4+}$ (0.9%) at $T = 4$ K. (**a**) Excitation spectra for λ_{em} = 622 nm (red), 625 nm (green), 630 nm (blue) and 637 nm (orange); (**b**) Emission spectra for λ_{exc} = 460 nm (red), 462 nm (green), 467 nm (blue) and 485 nm (orange).

3.3. Thermal Quenching in $M_3AlF_6:Mn^{4+}$

For high-power w-LED applications, the thermal quenching behavior of a phosphor is very important, as the temperature of the on-chip phosphor layer in a high-power w-LED reaches temperatures as high as 450 K. The thermal quenching behavior of $K_3AlF_6:Mn^{4+}$ and $Na_3AlF_6:Mn^{4+}$ has been investigated by Song et al. [17,18]. They reported that thermal quenching sets in around 423 K (150 °C) for $K_3AlF_6:Mn^{4+}$ and $Na_3AlF_6:Mn^{4+}$. More interestingly, they found that the integrated photoluminescence (PL) intensity of these phosphors doubles between room temperature and 423 K. This is a very useful property for high temperature applications, but is also very unexpected. For most Mn^{4+}-doped fluorides, the PL intensity is relatively constant between room temperature and the temperature at which thermal quenching sets in [8–10].

To investigate the thermal quenching of the Mn^{4+} emission in $M_3AlF_6:Mn^{4+}$ (M = Na, K), we measure the integrated PL intensity of $M_3AlF_6:Mn^{4+}$ as a function of temperature between 298 K and 600 K. Figure 6a shows emission spectra of $K_3AlF_6:Mn^{4+}$ recorded in this temperature range. Emission spectra of $Na_3AlF_6:Mn^{4+}$ and $K_2NaAlF_6:Mn^{4+}$ between 298 K and 600 K can be found in Figure S1. The results show that the PL intensity of $M_3AlF_6:Mn^{4+}$ slowly decreases up to 423 K (150 °C). Above this temperature, there is rapid quenching, with no emission intensity remaining at 573 K. After heating to 573 K, around half of the initial room-temperature PL intensity is retained. Part of the PL intensity is lost upon heating due to e.g., degradation of the phosphor, reduction/oxidation of the Mn^{4+} ions and formation of Mn-oxide impurities.

From the emission spectra recorded between 298 K and 600 K we obtain the temperature dependence of the integrated PL intensity (I_{PL}), which is displayed in Figure 6b. The intensity is given relative to the integrated PL intensity at room temperature (I_{RT}). The PL intensity gradually decreases between 300 K

and 450 K, but then at higher temperatures rapidly drops due to an increased probability for non-radiative transitions from the ^{2}E excited state (luminescence quenching). The luminescence quenching temperature $T_{1/2}$, the temperature at which the PL intensity is half of its initial value, is around 460 K for K_3AlF_6:Mn^{4+} and Na_3AlF_6:Mn^{4+} and 485 K for K_2NaAlF_6:Mn^{4+}. The $T_{1/2}$ values fall in the range of quenching temperatures reported for Mn^{4+}-doped fluoride phosphors [39,47]. The quenching temperatures of M_3AlF_6:Mn^{4+} are above the phosphor operating temperatures of high-power w-LEDs.
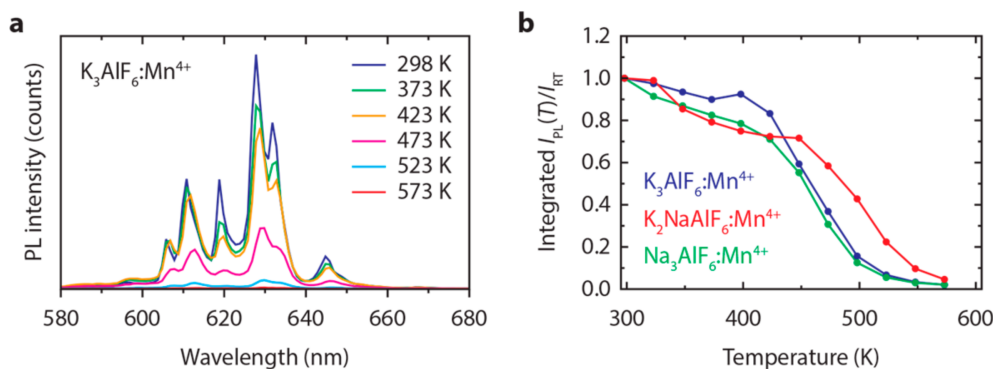
Figure 6. (**a**) Emission spectra of K_3AlF_6:Mn^{4+} (1.2%) at various temperatures between 298 K and 573 K (λ_{exc} = 450 nm); (**b**) Integrated PL intensity of K_3AlF_6:Mn^{4+} (1.2%) (blue), Na_3AlF_6:Mn^{4+} (0.4%) (green) and K_2NaAlF_6:Mn^{4+} (0.9%) (red) as a function of temperature between 300 and 600 K. The integrated PL intensity I_{PL} is scaled to the integrated PL intensity at room temperature I_{RT}.

The temperature dependences we obtain for K_3AlF_6:Mn^{4+} and Na_3AlF_6:Mn^{4+} (Figure 6b) are significantly different from the work by Song et al. [17,18]. We observe a small decrease in the P intensity between 298 K and 423 K, while they reported a doubling of the PL intensity between these temperatures. The decrease in PL intensity between 298 K and 423 K for M_3AlF_6:Mn^{4+} we ascribe to an increase of the energy transfer from Mn^{4+} ions to quenching sites (defects and impurities) with temperature [48]. The rapid quenching of the Mn^{4+} luminescence above 430 K is attributed to thermally activated crossing of the Mn^{4+} $^4T_2$ excited state and $^4A_2$ ground state, as is explained in [49].

Finally, we observe some interesting changes in the emission spectrum of K_2NaAlF_6:Mn^{4+} upon heating to 573 K. This is illustrated in Figure 7, which displays emission spectra recorded at T = 4 K and 298 K of K_2NaAlF_6:Mn^{4+} (0.9%) for as-synthesized K_2NaAlF_6:Mn^{4+} (blue spectra) and K_2NaAlF_6:Mn^{4+} phosphor that was heated to 573 K (red spectra). The room-temperature spectra in Figure 7a show that the structure of the $^2E \rightarrow {}^4A_2$ ZPL emission in K_2NaAlF_6:Mn^{4+} changes upon heating to 573 K. This effect is even more pronounced in the spectra measured at 4 K (Figure 7b). Four ZPLs of similar intensity are observed for the as-synthesized phosphor, while two ZPLs dominate the spectrum after heating at 573 K. In addition, the results in Figure 7b show that heating to 573 K changes the structure and intensity of the vibronic $^2E \rightarrow {}^4A_2$ emission lines. The changes in the emission spectra can be caused by a phase transition in the K_2NaAlF_6 crystal structure. However, the XRD patterns of as-synthesized K_2NaAlF_6:Mn^{4+} and K_2NaAlF_6:Mn^{4+} phosphor heated to 573 K both match the reference pattern of elpasolite K_2NaAlF_6, which indicates that no phase transition occurs (see Figure S2). We therefore explain the changes in the emission spectra upon high temperature annealing by a rearrangement of the Mn^{4+} sites in K_2NaAlF_6:Mn^{4+} upon heating to 573 K. Furthermore, the fact that two ZPLs dominate the emission spectrum of K_2NaAlF_6:Mn^{4+} after heating indicates that there is a redistribution in the abundance of different charge compensated Mn^{4+} sites. The results presented in Figure 7 show that post-synthesis heating can have a large effect on the luminescence properties of M_3AlF_6:Mn^{4+} and other Mn^{4+}-doped fluoride phosphors.
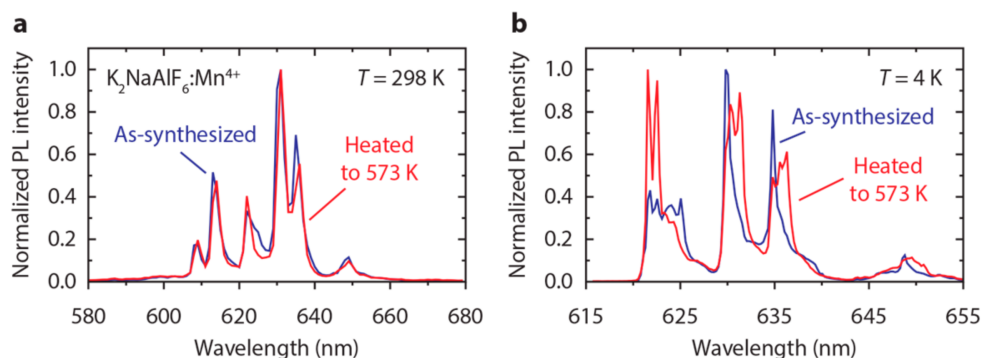
Figure 7. (**a**) Room-temperature emission spectra (λ_{exc} = 450 nm) of K_2NaAlF_6:Mn^{4+} (0.9%) for as-synthesized K_2NaAlF_6:Mn^{4+} phosphor (blue) and K_2NaAlF_6:Mn^{4+} phosphor that has been heated to 573 K (red); (**b**) Emission spectra of K_2NaAlF_6:Mn^{4+} (0.9%) at T = 4 K (λ_{exc} = 460 nm) for as-synthesized K_2NaAlF_6:Mn^{4+} phosphor (blue) and K_2NaAlF_6:Mn^{4+} phosphor that has been heated to 573 K (red).

4. Conclusions

Mn^{4+}-doped fluorides have recently attracted considerable attention due to their potential for application in w-LEDs. For application in w-LEDs, it is important to understand and control the synthesis and luminescence properties of Mn^{4+}-doped fluoride phosphors. Here, we report the synthesis of different M_3AlF_6:Mn^{4+} (M = Na, K) phosphors via a simple two-step co-precipitation method. Our synthesis method provides good control over Mn^{4+} doping and yields highly monodisperse ~20 μm smoothed octahedron shaped crystallites for K_2NaAlF_6:Mn^{4+}, while irregularly shaped particles with a broad size distribution are obtained for K_3AlF_6:Mn^{4+} and Na_3AlF_6:Mn^{4+}. All synthesized M_3AlF_6:Mn^{4+} phosphors show narrow red Mn^{4+} $^2E \rightarrow {}^4A_2$ luminescence that can be excited in the UV and blue spectral region. Luminescence spectra recorded at T = 4 K reveal that multiple Mn^{4+} sites are present in M_3AlF_6:Mn^{4+}, which was not observed in previous reports. The presence of multiple Mn^{4+} sites is attributed to charge compensation that is required for Mn^{4+} on Al^{3+} sites. The results show that charge compensating defects have a large influence on the luminescence properties (e.g., spectra, QY, luminescence lifetime) of Mn^{4+}-doped fluorides. Lowering of the QY by defect quenching is a problem for application of this class of Mn^{4+} phosphors. Finally, we investigated the thermal quenching behavior for M_3AlF_6:Mn^{4+}. The luminescence quenching temperature of M_3AlF_6:Mn^{4+} is between 460 K and 490 K, which is above the phosphor operating temperature in high-power w-LEDs. If the QY can be improved by suppressing defect quenching, Mn^{4+}-doped hexafluoroaluminates are a promising class of materials as their chemical and thermal stability is superior to the presently used commercial Mn^{4+} phosphors.

Author Contributions: Tim Senden and Andries Meijerink conceived and designed the experiments; Tim Senden and Robin G. Geitenbeek synthesized the phosphor particles; Tim Senden performed the characterization measurements; Tim Senden, Robin G. Geitenbeek and Andries Meijerink analyzed the data; Tim Senden and Andries Meijerink wrote the manuscript.

Conflicts of Interest: The authors declare no conflict of interest.

References

1. Charge of the LED brigade: A global switch to LEDs will change the lighting business. *Economist*. 2011. http://www.economist.com/node/21526373..

2. Krames, M.R.; Shchekin, O.B.; Mueller-Mach, R.; Mueller, G.O.; Zhou, L.; Harbers, G.; Craford, M.G. Status and future of high-power light-emitting diodes for solid-state lighting. *IEEE/OSA J. Disp. Technol.* **2007**, *3*, 160–175. [CrossRef]

3. Harbers, G.; Bierhuizen, S.J.; Krames, M.R. Performance of high power light emitting diodes in display illumination applications. *IEEE/OSA J. Disp. Technol.* **2007**, *3*, 98–109. [CrossRef]

4. Nakamura, S. Current status of GaN-based solid-state lighting. *MRS Bull.* **2009**, *34*, 101–107. [CrossRef]

5. Smet, P.F.; Parmentier, A.B.; Poelman, D. Selecting conversion phosphors for white light-emitting diodes. *J. Electrochem. Soc.* **2011**, *158*, R37–R54. [CrossRef]

6. Setlur, A.A. Phosphors for LED-based solid-state lighting. *Electrochem. Soc. Interface* **2009**, *18*, 32–36.

7. Xie, R.J.; Hirosaki, N. Silicon-based oxynitride and nitride phosphors for white LEDs—A review. *Sci. Technol. Adv. Mater.* **2007**, *8*, 588–600. [CrossRef]

8. Zhu, H.; Lin, C.C.; Luo, W.; Shu, S.; Liu, Z.; Liu, Y.; Kong, J.; Ma, E.; Cao, Y.; Liu, R.-S.; et al. Highly efficient non-rare-earth red emitting phosphor for warm white light-emitting diodes. *Nat. Commun.* **2014**, *5*, 4312. [CrossRef] [PubMed]

9. Setlur, A.A.; Radkov, E.V.; Henderson, C.S.; Her, J.-H.; Srivastava, A.M.; Karkada, N.; Kishore, M.S.; Kumar, N.P.; Aesram, D.; Deshpande, A.; et al. Energy-efficient, high-color-rendering LED lamps using oxyfluoride and fluoride phosphors. *Chem. Mater.* **2010**, *22*, 4076–4082. [CrossRef]

10. Sijbom, H.F.; Joos, J.J.; Martin, L.I.D.J.; Van den Eeckhout, K.; Poelman, D.; Smet, P.F. Luminescent behavior of the K_2SiF_6:Mn^{4+} red phosphor at high fluxes and at the microscopic level. *ECS J. Solid State Sci. Technol.* **2016**, *5*, R3040–R3048. [CrossRef]

11. Lin, C.C.; Meijerink, A.; Liu, R.-S. Critical red components for next-generation white LEDs. *J. Phys. Chem. Lett.* **2016**, *7*, 495–503. [CrossRef] [PubMed]

12. Nguyen, H.-D.; Liu, R.-S. Narrow-band red-emitting Mn^{4+}-doped hexafluoride phosphors: Synthesis, optoelectronic properties, and applications in white light-emitting diodes. *J. Mater. Chem. C* **2016**, *4*, 10759–10775. [CrossRef]

13. Hoshino, R.; Adachi, S. Photo-induced degradation and thermal decomposition in $ZnSnF_6 \cdot 6H_2O$:Mn^{4+} red-emitting phosphor. *Opt. Mater.* **2015**, *48*, 36–43. [CrossRef]

14. Sijbom, H.F.; Verstraete, R.; Joos, J.J.; Poelman, D.; Smet, P.F. K_2SiF_6:Mn^{4+} as a red phosphor for displays and warm-white LEDs: A review of properties and perspectives. *Opt. Mater. Express* **2017**, *7*, 3332–3365. [CrossRef]

15. Murphy, J.E.; Garcia-Santamaria, F.; Setlur, A.A.; Sista, S. PFS, K_2SiF_6:Mn^{4+}: The red-line emitting LED phosphor behind GE's TriGain Technology^{TM} platform. *SID Symp. Dig. Tech. Pap.* **2015**, *46*, 927–930. [CrossRef]

16. Nguyen, H.-D.; Lin, C.C.; Liu, R.-S. Waterproof alkyl phosphate coated fluoride phosphors for optoelectronic materials. *Angew. Chem. Int. Ed.* **2015**, *54*, 10862–10866. [CrossRef] [PubMed]

17. Song, E.H.; Wang, J.Q.; Ye, S.; Jiang, X.F.; Peng, M.Y.; Zhang, Q.Y. Room-temperature synthesis and warm-white LED applications of Mn^{4+} ion doped fluoroaluminate red phosphor Na_3AlF_6:Mn^{4+}. *J. Mater. Chem. C* **2016**, *4*, 2480–2487. [CrossRef]

18. Song, E.; Wang, J.; Shi, J.; Deng, T.; Ye, S.; Peng, M.; Wang, J.; Wondraczek, L.; Zhang, Q. Highly efficient and thermally stable K_3AlF_6:Mn^{4+} as a red phosphor for ultra-high-performance warm white light-emitting diodes. *ACS Appl. Mater. Interfaces* **2017**, *9*, 8805–8812. [CrossRef] [PubMed]

19. Zhu, Y.; Cao, L.; Brik, M.G.; Zhang, X.; Huang, L.; Xuan, T.; Wang, J. Facile synthesis, morphology and photoluminescence of a novel red fluoride nanophosphor K_2NaAlF_6:Mn^{4+}. *J. Mater. Chem. C* **2017**, *5*, 6420–6426. [CrossRef]

20. Zhu, Y.; Huang, L.; Zou, R.; Zhang, J.; Yu, J.; Wu, M.; Wang, J.; Su, Q. Hydrothermal synthesis, morphology and photoluminescent properties of an Mn^{4+}-doped novel red fluoride phosphor elpasolite K_2LiAlF_6. *J. Mater. Chem. C* **2016**, *4*, 5690–5695. [CrossRef]

21. Shannon, R.D. Revised effective ionic radii and systematic studies of interatomic distances in halides and chalcogenides. *Acta Crystallogr. Sect. A* **1976**, *32*, 751–767. [CrossRef]

22. Thompson, W.T.; Goad, D.G.W. Some thermodynamic properties of K$_3$AlF$_6$–KAlF$_4$ melts. *Can. J. Chem.* **1976**, *54*, 3342–3349. [CrossRef]

23. Rumble, J.R. *Handbook of Chemistry and Physics*, 98th ed.; CRC Press: Boca Raton, FL, USA; Taylor & Francis: Boca Raton, FL, USA, 2017.

24. Lv, L.; Jiang, X.; Huang, S.; Chen, X.; Pan, Y. The formation mechanism, improved photoluminescence and LED applications of red phosphor K$_2$SiF$_6$:Mn^{4+}. *J. Mater. Chem. C* **2014**, *2*, 3879–3884. [CrossRef]

25. Setlur, A.A.; Lyons, R.J.; Nammalwar, P.K.; Hanumanlha, R.; Murphy, J.E.; Garcia, F. Moisture-Resistant Phosphor Compositions and Associate Methods. World Patent WO 2,015,102,876, 9 July 2015.

26. Shriver, D.F.; Atkins, P.W. *Inorganic Chemistry*, 4th ed.; Oxford University Press: Oxford, UK, 2006.

27. Bode, H.; Jenssen, H.; Bandte, F. Über eine neue darstellung des kalium-hexafluoromanganats (IV). *Angew. Chem.* **1953**, *65*, 304. [CrossRef]

28. Roesky, H.W. *Efficient Preparations of Fluorine Compounds*; Roesky, H.W., Ed.; John Wiley & Sons Inc.: Hoboken, NJ, USA, 2012; ISBN 9781118409466.

29. Morss, L.R. Crystal structure of dipotassium sodium fluoroaluminate (elpasolite). *J. Inorg. Nucl. Chem.* **1974**, *36*, 3876–3878. [CrossRef]

30. Hawthorne, F.C.; Ferguson, R.B. Refinement of the crystal structure of cryolite. *Can. Mineral.* **1975**, *13*, 377–382.

31. Abakumov, A.M.; King, G.; Laurinavichute, V.K.; Rozova, M.G.; Woodward, P.M.; Antipov, E.V. The crystal structure of α-K$_3$AlF$_6$: Elpasolites and double perovskites with broken corner-sharing connectivity of the octahedral framework. *Inorg. Chem.* **2009**, *48*, 9336–9344. [CrossRef] [PubMed]

32. Adachi, S.; Takahashi, T. Photoluminescent properties of K$_2$GeF$_6$:Mn^{4+} red phosphor synthesized from aqueous HF/KMnO$_4$ solution. *J. Appl. Phys.* **2009**, *106*, 013516. [CrossRef]

33. Xu, Y.K.; Adachi, S. Properties of Na$_2$SiF$_6$:Mn^{4+} and Na$_2$GeF$_6$:Mn^{4+} red phosphors synthesized by wet chemical etching. *J. Appl. Phys.* **2009**, *105*, 013525. [CrossRef]

34. Jiang, X.; Pan, Y.; Huang, S.; Chen, X.; Wang, J.; Liu, G. Hydrothermal synthesis and photoluminescence properties of red phosphor BaSiF$_6$:Mn^{4+} for LED applications. *J. Mater. Chem. C* **2014**, *2*, 2301–2306. [CrossRef]

35. Fang, M.-H.; Nguyen, H.-D.; Lin, C.C.; Liu, R. Preparation of a novel red Rb$_2$SiF$_6$:Mn^{4+} phosphor with high thermal stability through a simple one-step approach. *J. Mater. Chem. C* **2015**, *3*, 7277–7280. [CrossRef]

36. Zhou, Q.; Tan, H.; Zhou, Y.; Zhang, Q.; Wang, Z.; Yan, J.; Wu, M. Optical performance of Mn^{4+} in a new hexa-coordinative fluorozirconate complex of Cs$_2$ZrF$_6$. *J. Mater. Chem. C* **2016**, *4*, 7443–7448. [CrossRef]

37. Wang, Z.; Zhou, Y.; Yang, Z.; Liu, Y.; Yang, H.; Tan, H.; Zhang, Q.; Zhou, Q. Synthesis of K$_2$XF$_6$:Mn^{4+} (X = Ti, Si and Ge) red phosphors for white LED applications with low-concentration of HF. *Opt. Mater.* **2015**, *49*, 235–240. [CrossRef]

38. De Mello Donegá, C. Synthesis and properties of colloidal heteronanocrystals. *Chem. Soc. Rev.* **2011**, *40*, 1512–1546. [CrossRef] [PubMed]

39. Paulusz, A.G. Efficient Mn(IV) emission in fluorine coordination. *J. Electrochem. Soc.* **1973**, *120*, 942–947. [CrossRef]

40. Takahashi, T.; Adachi, S. Mn^{4+}-activated red photoluminescence in K$_2$SiF$_6$ phosphor. *J. Electrochem. Soc.* **2008**, *155*, E183–E188. [CrossRef]

41. Senden, T.; Broers, F.T.H.; Meijerink, A. Comparative study of the Mn^{4+} ^{2}E $\rightarrow$ ^{4}A$_2$ luminescence in isostructural RE$_2$Sn$_2$O$_7$:Mn^{4+} pyrochlores (RE^{3+} = Y^{3+}, Lu^{3+} or Gd^{3+}). *Opt. Mater.* **2016**, *60*, 431–437. [CrossRef]

42. Blasse, G.; Grabmaier, B.C. *Luminescent Materials*; Springer: Berlin, Germany, 1994.

43. Garcia-Santamaria, F.; Murphy, J.E.; Setlur, A.A.; Sista, S.P. Concentration quenching in K$_2$SiF$_6$:Mn^{4+} phosphors. *ECS J. Solid State Sci. Technol.* **2018**, *7*, R3030–R3033. [CrossRef]

44. Chodos, S.L.; Black, A.M.; Flint, C.D. Vibronic spectra and lattice dynamics of Cs$_2$MnF$_6$ and A^1$_2$M^{IV}F$_6$:MnF$_6$$^{2-}$. *J. Chem. Phys.* **1976**, *65*, 4816–4824. [CrossRef]

45. Brik, M.G.; Srivastava, A.M. On the optical properties of the Mn^{4+} ion in solids. *J. Lumin.* **2013**, *133*, 69–72. [CrossRef]

46. Brik, M.G.; Camardello, S.J.; Srivastava, A.M. Influence of covalency on the Mn^{4+} ^{2}E$_g$ $\rightarrow$ ^{4}A$_{2g}$ emission energy in crystals. *ECS J. Solid State Sci. Technol.* **2014**, *4*, R39–R43. [CrossRef]

47. Sakurai, S.; Nakamura, T.; Adachi, S. Rb$_2$SiF$_6$:Mn^{4+} and Rb$_2$TiF$_6$:Mn^{4+} red-emitting phosphors. *ECS J. Solid State Sci. Technol.* **2016**, *5*, R206–R210. [CrossRef]

48. Bachmann, V.; Ronda, C.; Meijerink, A. Temperature quenching of yellow Ce^{3+} luminescence in YAG:Ce. *Chem. Mater.* **2009**, *21*, 2077–2084. [CrossRef]

49. Senden, T.; van Dijk-Moes, R.J.A.; Meijerink, A. Quenching of the red Mn^{4+} luminescence in Mn^{4+}-doped fluoride LED phosphors. *ECS J. Solid State Sci. Technol.* **2017**. Unpublished work.